Correction of static and thermal aberrations of a zigzag slab amplifier employing a wave-front sensor-less adaptive optics system

Ping Yang (杨 平)[1,2*], Bing Xu (许 冰)[1,2], Xiang Lei (雷 翔)[1,2], and Lizhi Dong (董理治)[1,2]

[1] *The Key Laboratory on Adaptive Optics, Chinese Academy of Sciences, Chengdu 610209, China*

[2] *Institute of Optics and Electronics, Chinese Academy of Sciences, Chengdu 610209, China*

[*] *Corresponding author: pingyang2516@163.com*

Received April 5, 2012; accepted September 4, 2012; posted online November 23, 2012

We present a wave-front sensor-less adaptive optics (AO) system for a Nd:YAG Zigzag slab amplifier. A 39-element rectangular piezoelectric deformable mirror in combination with a stochastic parallel gradient descent (SPGD) algorithm is introduced for both static and thermal aberrations correction. Preliminary experiments demonstrate that the output beam quality can be enhanced greatly at different power levels.

OCIS codes: 140.3280, 010.1080, 230.4040.

doi: 10.3788/COL201210.S21409.

Zigzag slab laser amplifier is promising laser architecture for achieving high power and high quality beam output. Compared with its counterparts such as rod lasers, disc lasers, the distortions generated in the zigzag slab are much smaller at the same power level due to its better cooling means and convenient thermal management. However, it is should also be noted that many detrimental factors, such as thermally induced strain and distortions, static aberrations from the optical components and so on, would induce wave-front distortions in the laser field and reduce the output beam quality. Therefore, many researchers have been engaging in developing techniques to improve the performance of zigzag slab amplifiers to the best of their ability[1−4]. Generally, it is difficult to compensate for all the wave-front distortions generated in the slab laser just through passive methods, especially for those dynamic thermal distortions. To offer a promising alternative, we employ the active method based on adaptive optics (AO) to correct the distortions in a zigzag slab amplifier. This AO system mainly includes a 39-element rectangular deformable mirror (DM), a far-field detector, and a stochastic parallel gradient descent (SPGD) optimization algorithm. What is different from those conventional AO systems used in many fields is that this wave-front sensor-less SPGD AO system does not need any wave-front sensors to measure wave-front information, but use the far-field metric which is mainly determined by the beam quality to control the DM and achieve distortions correction. This strategy is low cost and compact to implement in the zigzag slab amplifier system.

The optical layout of the AO system for beam cleanup of the slab amplifier is shown in Fig. 1. It has a master-oscillator-power-amplifier (MOPA) configuration. The seed laser is Nd:YAG continuous wave (CW) laser with a wavelength of 1 064 nm and a 1.3-W Gaussian mode output. The seed beam passes through an isolator and a 4-X expander to form a Φ2 mm beam, and then its size will be transformed into 1.8×10 (mm) by a cylinder expander (CE) and a slim at the entrance end of the slab amplifier. The thin rectangular laser crystal has a size of 67×11×1.8 (mm) and can be pumped by two offset bars on either side of the crystal. The beam can pass through the slab amplifier 4 times (for convenience, many optical elements for making the beam's 4 times passing through the slab is not given in the schematic) and the largest gain ratio of the slab amplifier is 300. At the exit end of the amplifier, the dimension of the beam is 1.9×10 (mm). Two cylinder expanders (CY and CX) in two orthogonal directions are used in turn to convert the beam size to 28×20 (mm) for making use of the effective area of DM. The DM employed in this system is a rectangular piezoelectric DM with 39 actuators. This DM fabricated in our lab has the following parameters: effective area of 40×40 (mm), stroke range of ±3 μm, maximum voltage of ±500 V, damage-threshold of >2 kW/cm^2. The photograph of the DM and the spatial configuration of laser beam and the DM are shown in Fig. 2.

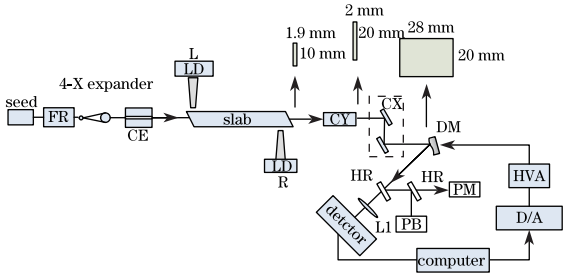

Fig. 1. Schematic of the experimental system.

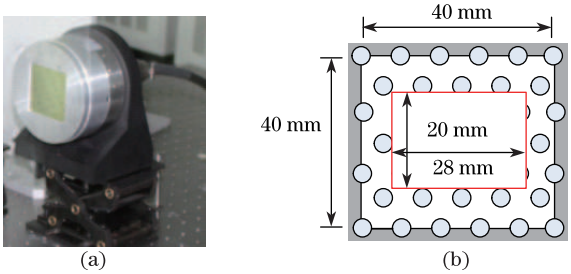

Fig. 2. (a) Photograph and (b) actuators configuration of the 39-element rectangular DM, respectively. Circles represent the actuators and the rectangle shows the size of incident laser beam.

 © 2012 Chinese Optics Letters

After reflected by the DM, the beam is incident on a high reflector (HR). The reflective part is collected by a power meter (PM) and a power bucket (PB) while the transmitted branch goes to a high-speed CMOS detector through a lens (L1) with a focal length of 300 mm. The power-in-a-bucket (PIB) of far-field spot on the CMOS is used as the performance metric of SPGD algorithm. The performance metric acquired through the complementary metal-oxide semiconductor (CMOS) detector is fed into the industrial computer-based SPGD controller through a built-in analay-to-digital (A/D) converter board. The SPGD algorithm firstly produces the updating 39 digital control voltages, and then outputs the voltages through a D/A converter board. A D/A converter and a multi-channel high-voltage-amplifier (HVA) transform and amplify the voltages to 39 analog voltages in turn to the range [–500-V, 500-V]. At last, these analog voltages are loaded on the 39 actuators of the DM to maximize the performance metric and compensate for the distortions introduced by the slab amplifiers.

The basic principle of SPGD algorithm has been demonstrated in many papers[5,6], here, we just present its application in the distortions correction experiments briefly. Using $J = J(u_1, u_2, \cdots, u_{39})$ as the performance function[7], of which u_1, u_2, $\cdots$, u_{39} are the voltages applied on the DM. Each iteration calculation works as follows. 1) Firstly, produce a group of statistically independent random perturbations with small amplitude, $\delta u_1, \delta u_2, \cdots, \delta u_{39}$; 2) then apply the voltages $u_1, u_2, \cdots, u_{39}$ in combination with the positive perturbations onto the 39 actuators of the DM and evaluate the positive performance metric: $J_+ = J(u_1 + \delta u_1, u_2 + \delta u_2, \cdots, u_{39} + \delta u_{39})$; 3) and then, apply the voltages $u_1, u_2, \cdots, u_{39}$ and the negative perturbations onto the 39 actuators of the DM and evaluate the negative performance metric: $J_- = J(u_1 - \delta u_1, u_2 - \delta u_2, \cdots, u_{39} - \delta u_{39})$; 4) calculate the difference between the two performance metrics: $\delta J = J_+ - J_-$t; 5) update voltages as: $u_i = u_i + \gamma \delta u_i \delta J$, $i = 1$ to 39, where γ is the gain coefficient.

The above steps repeats until the performance metric reach its maximum. Since the SPGD algorithm needs iterative calculation, thus, the AO system based on SPGD requires high operational bandwidth. Due to the high speed CMOS employed in this system, the maximum iterative rate for the SPGD algorithm is larger than 1000 iteration per second which offers the possibility for compensating for both the static and thermal dynamic aberrations.

The experiment for compensation of the static aberrations is presented. The seed laser passes through the entire beam path and brings out the static aberrations which come from the optical components, the slab and so on. The amplifier is not pumped during the static compensation stage. The β factor[8] is one of the important criterions for evaluating the beam quality. There are many ways to define the β factor, while the β factor in this letter is defined as the ratio of the far-field divergence angle of the measured beam to that of the ideal beam in the same diffraction-limited area. Generally, the smaller the β factor, the more the far-field energy contained within the appointed area, and the ideal β factor is 1. As shown in Figs. 3 and 4, when the AO system is switched on, more energy is assembled in the centre of the camera and the peak intensity is increased from 25 to 125 (0∼255). The β factor is reduced from 4.5 to 2.3.

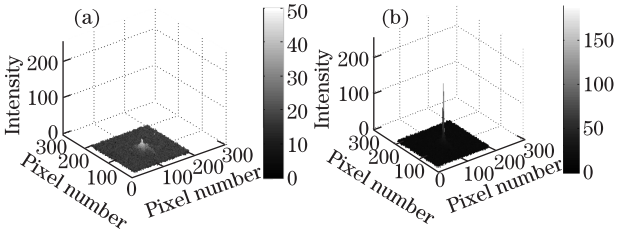

Fig. 3. Three-dimensional (3D) distributions of far-field laser spots. (a) Open-loop case; (b) close-loop case.

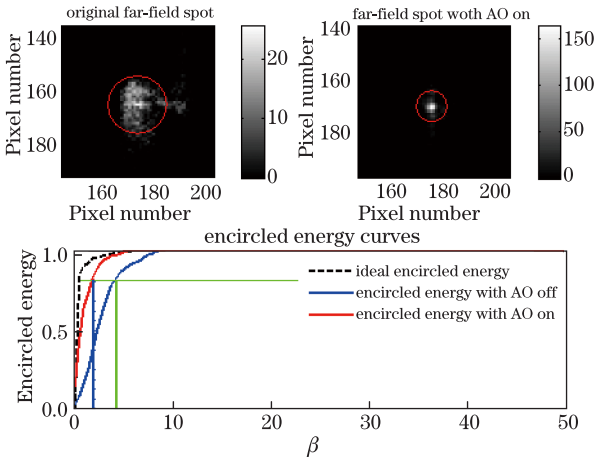

Fig. 4. Far-field distributions and encircled energy curves at static aberrations correction case, the two circles in top two plots contain 84% energy of the total far-field energy of both open-loop and close-loop cases.

During many factors for reducing beam quality of zigzag slab amplifiers, thermal aberrations (especially in the case of relative high output) may play one of the most prominent roles. Therefore, they have to be compensated for achieving promising beam quality. As for the amplifier system described in this letter, the slab crystal can be pumped by left or right bars on either end of the crystal or by both bars simultaneously.

We firstly let the zigzag slab amplifier work under the left end pumping and do not allow right bars to operate. Although the pumping current can be adjusted continually from 0 to 80 A, however, a work point is clear enough for demonstrating the correction capability of this AO system; therefore, we just set the pumping current at its maximum value, i.e. 80 A (corresponding to 63-W output). Experimental correction result is shown in Fig. 5. We can see that after the AO system is switched on, the peak light gray intensity is improved from 75 to 180, the large spread light spot become a small bright one and the calculated β factor is reduced greatly from 17.6 to 5.9.

And then, we only let the amplifier work at right end pumping and the pumping current is also set at 80 A which corresponds to 73-W output. Figure 6 shows the correction performance, the peak intensity is also increased greatly when AO system works. The far-field

distributions and encircled energy curves in the case of right end pumping are shown in Fig. 7. The top left plot is the original far-field spot with AO system off (open-loop) while the top right plot is the far-field spot with AO system switching on (close-loop). In both plots, the fraction of the total energy contained within the red circle is 84%. The bottom plot shows the encircled energy curves of which the X-coordinate represents the times of diffraction-limited area, and the Y-coordinate represents encircled energy. What we can know from the bottom plot is that when the SPGD AO system is switched on, the β factor is brought down to 4.9 from 13.5. This obvious improvement can be attributed to the effective compensation of the aberrations (including both the thermal and static aberrations).

Compared the original and corrected far-field spots in left end pumping with those of right end pumping, we can find that they are different from each other. Two main reasons may explain this phenomenon, one is due to the diode bars on both end are not the same, as a result the pumping beam quality generated by them isnot equal, therefore the output beam quality cannot be the same, on the other hand, two pumping beams may not go through just the same slab amplifier path due to the optical installation errors and the incident angles errors, therefore, the output beam quality and output power on two cases are not the same although they both work at the pumping current of 80 A.

More often than not, this slab amplifier is worked by two ends pumping. Let two pumping bars work at 80 A, the output power now can reach 265 W. As shown in Fig. 8, after correction, the peak intensity is increased

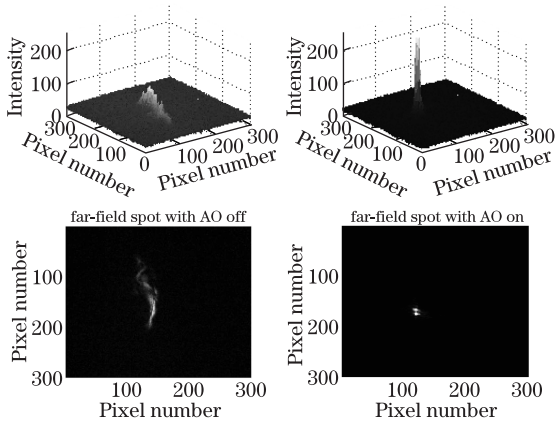

Fig. 5. Distributions of far-field spots at left end pumping case. Left two plots represent the open–loop case while the right two plots show the close-loop case.

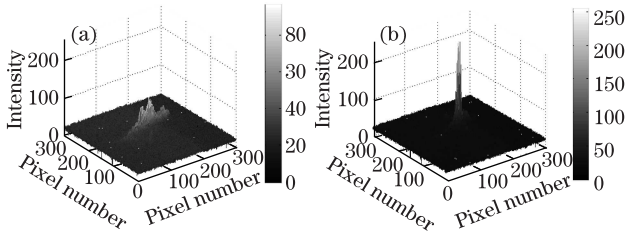

Fig. 6. 3D intensity distributions of far-field focal spots at right end pumping case. (a) open-loop case; (b) close-loop case.

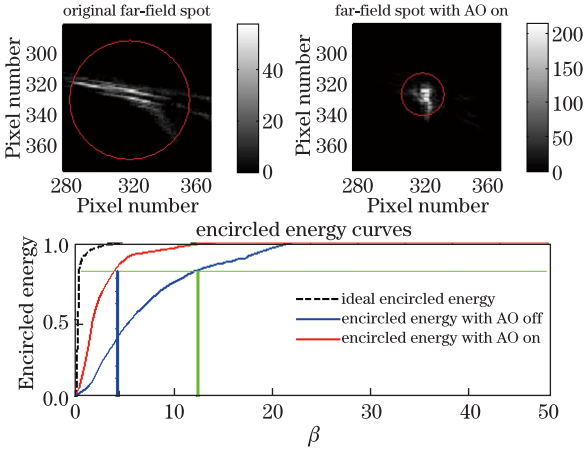

Fig. 7 Far-field distributions and the encircled energy curves at right end pumping case.

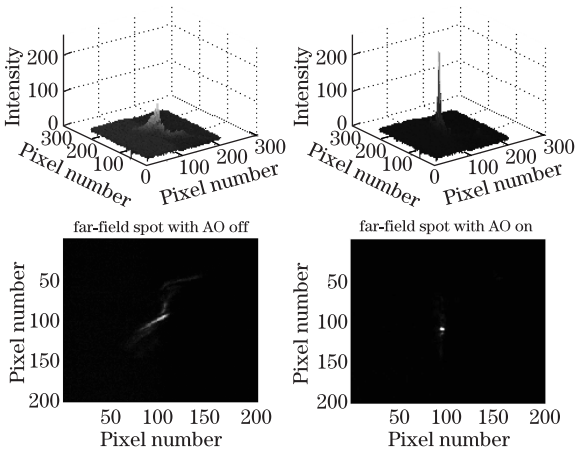

Fig. 8 Far-field pattern distributions at 265-W output. Left two plots represent the open-loop case while the right two plots show the close-loop case.

prominently, besides we can also figure out that the β factor has been brought down to 6.2 from 15.5.

In conclusion, we present a wave-front sensor-less SPGD AO system for compensating the aberrations of zigzag slab amplifiers. Experimental results indicate that both the static and thermal dynamic aberrations in the amplifiers can be corrected effectively. Although the obtained results are far from the diffraction-limited, however, we prove that this AO system is capable of correcting the aberrations in the slab amplifier. For obtaining a better correction performance, designing a higher spatial precision DM and a more appropriate cylinder system for matching the beam aperture and the DM's size better is developing.

This work was supported by the National Natural Science Foundation of China (Nos. 10974202, 60978049), Sichuan Outstanding Youth Science Foundation, and the Innovation Foundation of Chinese Academy of Sciences (Nos. 2012JQ0012, A09K005, and CXJJ-10-S01).

References

1. K. Du, N. Wu, J. Xu, J. Giesekus, P. Loosen, and R. Poprawe, Opt. Lett. **23,** 370 (1998).

2. H. Baker, A. A. Chesworth, D. Pelaez Millas, and D. R. Hall, Opt. Commum. **191,** 125 (2001).
3. J. M. Eggleston, T. J. Kane, K. Kuhn, J. Unternahrer, and R. L. Byer, IEEE J. Quantum Electron. **QE-20,** 289 (1984).
4. M. Ostermeyer, D. Mudge, P. J. Veitch, and J. Munch, Appl. Opt. **45,** 5368 (2006).
5. M. A. Vorontsov and V. P. Sivokon, J. Opt. Soc. Am. A **15,** 2745 (1998).
6. M. A. Vorontsov, G. W. Carhart, and J. C. Ricklin, Opt. Lett. **22,** 907 (1997).
7. L. Liu and M. A. Vorontsov, Proc. SPIE **5895,** 58950P-1 (2005).
8. P. Yang, Y. Liu, W. Yang, M. W. Ao, S. J. Hu, B. Xu, and W. H. Jiang, Opt. Commun. **278,** 377 (2007).